Suspended InGaAs Sub-Wavelength Grating Cladding Waveguide for Monolithic Integration with Quantum Cascade Lasers and Detectors for Mid-Infrared On-Chip Gas Sensing

Kyoung Min Yoo[1], Jason Midkiff[1], Chi-Jui Chung[1], Hamed Dalir[2] and Ray T. Chen[1,2]
[1]Department of Electrical and Computer Engineering, The University of Texas at Austin, 10100 Burnet Rd. Austin, TX, 78758, USA.
[2]Omega Optics Inc., 8500 Shoal Creek Blvd., Bldg. 4, Suite 200, Austin, TX, 78757, USA.
Author e-mail address: yoo_eb@utexas.edu

Abstract: Fully suspended InGaAs membrane sub-wavelength grating cladding waveguides (SWWs) are designed and fabricated for mid-infrared ammonia sensing at λ=6.15μm in the InGaAs-InP platform considering monolithic integration of quantum cascade devices with 84 ppb estimating sensitivity. © 2020 The Author(s)

Mid-IR trace-gas sensing is a vigorously developing field with a wide range of applications based on molecular absorption spectroscopy and the fundamental vibrational-rotational transitions of chemical bonds in the wavelength range between 3-20 μm. Specifically, the molecular fingerprint region (700-1500 cm^{-1}) contains many absorption bands related to bending and stretching of molecular skeleton modes that allow unique identification of chemical compounds with high sensitivity and specificity [1]. Recently, mid-IR absorption spectroscopy based on integrated photonic circuits has shown great promise in terms of light-weight, alignment-free, compact and high sensitivity. Especially, monolithic integration of light sources and detectors with passive photonics devices is required to enable a compact trace gas sensing system that is robust to vibrations and physical stress. Here, quantum cascade lasers (QCLs) have significantly affected the feasibility of integrated photonic circuits by providing narrowband tunable continuous-wave room-temperature emission source in the entire mid-IR spectral range from 3-11 μm. [2] To cover the entire molecular fingerprint region from λ=3-15μm, several low-loss material platforms such as Ge-GaAs, GaAs-AlGaAs, InGaAs-InP have been demonstrated [1,3]; but only the $In_{0.53}Ga_{0.47}As$/InP platform allows monolithic epitaxial growth of QCL/QCDs and eliminates the expensive and low yield wafer/chip bonding processes and the need for intermediate adhesive layers such as SU8 (lossy at λ > 5 μm wavelength), silicon dioxide (lossy at λ > 3.7 μm). In this paper, targeting monolithic integration of QCL/QCDs and passive devices, we choose $In_{0.53}Ga_{0.47}As$/InP platform to fabricate passive waveguide devices. In recent years, sub-wavelength grating waveguides, or sub-wavelength meta-material clad waveguides, defined by a periodic array of rectangular holes bordering a strip waveguide, have been proposed as effective ways to ameliorate the cladding limitations, when appropriate high index core materials are available [4-6].

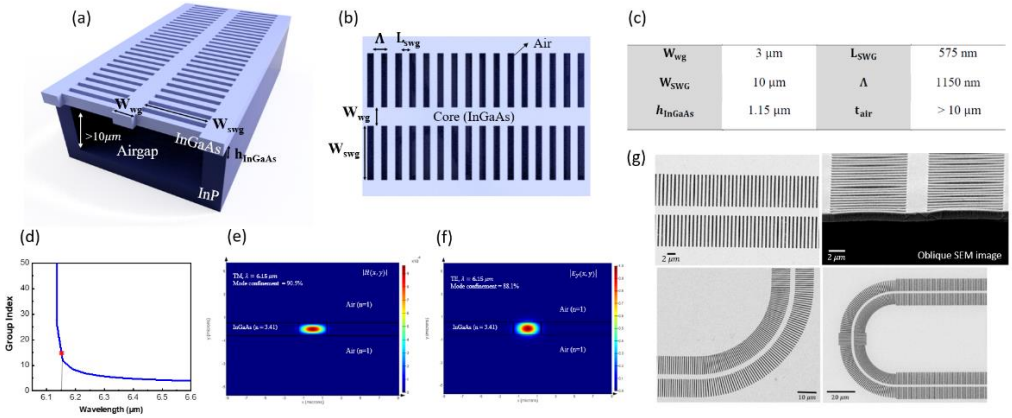

W_{wg}	3 μm	L_{SWG}	575 nm
W_{SWG}	10 μm	Λ	1150 nm
h_{InGaAs}	1.15 μm	t_{air}	> 10 μm

Fig. 1. (a) 3D schematic of suspended InGaAs SWW structure. (b) Top-view schematics of suspended InGaAs SWW. (c) The optimized dimensions of the suspened SWW. (d) Group index of SWW with the optimized dimensions in (c). (e) Cross-section of the fundamental TM mode profile and (f) TE mode profile at λ = 6.15 μm. (g) Top and oblique SEM images of fabricated devices including bending structures.

We designed the suspended InGaAs sub-wavelength grating cladding waveguides (SWWs), which have the suspended InGaAs strip defined between two SWG metamaterial claddings. Fig. 1. (a) shows the 3D schematic of a

suspended InGaAs SWW device structure and (b) shows the top-view schematics. To minimize the out-of-plane leakage due to the low refractive index contrast between InGaAs and InP (Δn~0.3), we etch away the InP substrate to build suspended membrane waveguides to ensure Δn~2.4. The lateral SWG claddings have an effective refractive index intermediate between the indices of InGaAs and air based on effective medium theory (EMT) [4]. In addition, they allow easy access of the wet etchant for the removal of the underlying InP cladding, as well as support for the InGaAs strip waveguide after being suspended. Light is index-guided in the InGaAs strip waveguide surrounded by the upper/lower air claddings and the lateral SWG claddings, and the structural slow-light is generated by modulating the index guided optical mode with SWG sidewalls along the propagation direction [4-6]. We optimized the lattice periodicity of SWG claddings to suppress reflection and diffraction effects and operate in the sub-wavelength regime by choosing a lattice periodicity that is less than half the Bragg period (Eq. 1) using Bloch-Floquet formalism: $\Lambda < \frac{1}{2}\frac{\lambda}{n_B}$ (1)

Fig. 1. (c) shows the optimized dimensions of the suspended SWW device for the fundamental TM mode at λ = 6.15 μm for ammonia sensing. Fig. 1. (d) shows the group index of suspended SWW with optimized dimensions with n_g = 14.8 at λ = 6.15 μm. Fig. 1. (e) and (f) show the mode simulations of the fundamental TM and TE modes at λ = 6.15 μm, respectively. Due to the high index contrast between the strip waveguide and the claddings, the SWW exhibits sufficient mode confinement to reduce the propagation loss. Moreover, both fundamental TM and TE modes are supported with 90.5% and 88.1% mode confinement in the waveguide, respectively. When we consider monolithic integrated circuits with QCL/QCD devices with TM polarized characteristics, these mode compatibilities provide the advantages of forgoing the total transmission loss from a polarization rotation splitter (which is necessary for 2D photonic crystal waveguide) and minimizing the device footprint.

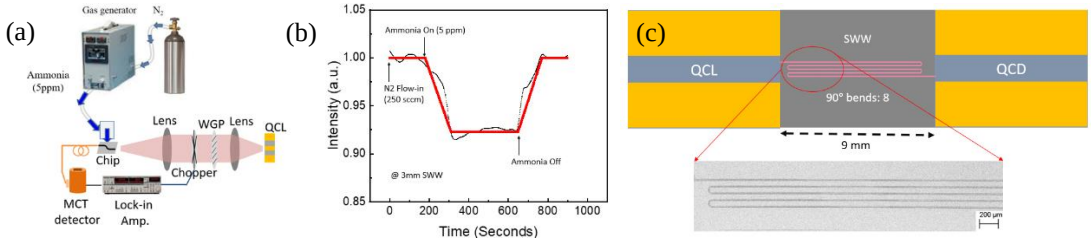

Fig. 2. (a) Schematic of gas sensing measurement setup. (b) 3mm long SWW device ammonia detection result at 5ppm with TM polarized light. (c) The schematic illustration of the envisioned top-view layout and corresponding SEM image of monolithic integrated sensors with SWW.

Fig. 1. (g) show top and cross (oblique) view SEM images of fabricated devices. The devices are cleaved and characterized with end-fire coupling setup as shown in Fig. 2. (a). By measuring the output power versus time, in the presence and absence of ammonia flow from a calibrated Kintek vapor generator, we successfully detected ammonia at 5ppm from 3mm SWW device with 7.7% signal drop, as shown in Fig. 2. (b). The slopes observed during ammonia On/Off are related to the lag time of ammonia flow from the vapor generator via tubing to the surface of our chip. Also, we measured the propagation loss of 4.1 dB/cm by cutback method. According to the Beer-Lambert law, absorptivity of the waveguide is given by: A= $\alpha\gamma LC$……..(2) where α is the absorption coefficient of the medium, L is the optical path length, C is the ammonia gas concentration and γ is the medium-specific absorption factor determined by dispersion enhanced light-matter interaction [7]. Here, we note the relationship between the optical path length and the gas concentration as: $C \propto \frac{1}{L}$……. (3), so the minimum detectable concentration decreases with longer SWW. We estimated the minimum sensitivity of monolithic integrated circuits based on the Beer-Lambert law and the performance of discrete components. Fig. 2. (c) shows the schematic illustration of top-view monolithic integrated sensors with SWW. The total transmission loss is limited as 20 dB due to the side mode suppression ratio of QCL device (Thorlabs QD6500CM1), and the minimum detectable concentration from 3mm SWW was ~1.26 ppm, so we estimate the minimum sensitivity of ~84 ppb from 44.9 mm long SWW, but the total length of the device footprint is about $\frac{44.9\ mm}{5} = 9\ mm$ as shown in Fig. 2. (c) with 8 0.2 dB loss 90° bends [8]. The research was supported by Army (ARO) SBIR Contract # W911NF-18-C-0085. The content of the information does not necessarily reflect the position or the policy of the Government, and no official endorsement should be inferred.

References

[1] Y. Zou, et al., Photon. Res. 6, 254-276 (2018).
[2] Y. Yao, et al., Nat. Photon. 6, 432-439 (2012).
[3] R. Soref, Nat. Photon. 4, 495-497 (2010).
[4] R. Halir, et al., Laser & Photon. Rev. 9, 25-49 (2015).
[5] J. H. Schmid, et al., IEEE Photon. J. 3, 597-607 (2011)
[6] C. -J. Chung, et al., App. Phys. Letters. 112, 071104 (2018)
[7] N. A. Mortensen, S. Xiao, App. Phys. Letters. 90, 141108 (2007)
[8] S. Chakravarty, et al., Proc. Spie. 10921 (2019)